Journal of Advanced Research 25 (2020) 57–66

Contents lists available at ScienceDirect

Journal of Advanced Research

journal homepage: www.elsevier.com/locate/jare

New fractional-order shifted Gegenbauer moments for image analysis and recognition

Khalid M. Hosny [a,*], Mohamed M. Darwish [b], Mohamed Meselhy Eltoukhy [c,d]

[a] Information Technology Department, Faculty of Computers and Informatics, Zagazig University, Zagazig 44519, Egypt
[b] Mathematics Department, Faculty of Science, Assiut University, Assiut 71516, Egypt
[c] Computer Science Department, Faculty of Computers and Informatics, Suez Canal University, Ismailia, Egypt
[d] College of Computing and Information Technology, Khulais, University of Jeddah, Saudi Arabia

GRAPHICAL ABSTRACT

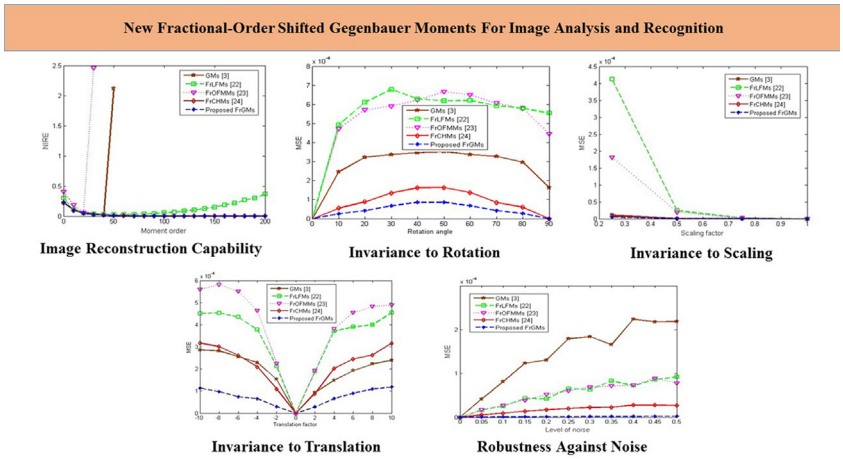

ARTICLE INFO

Article history:
Received 4 March 2020
Accepted 23 May 2020
Available online 1 June 2020

Keywords:
Fractional-order shifted Gegenbauer moments
Geometric transformations
Image recognition
Image analysis
Image reconstruction

ABSTRACT

Orthogonal moments are used to represent digital images with minimum redundancy. Orthogonal moments with fractional-orders show better capabilities in digital image analysis than integer-order moments. In this work, the authors present new fractional-order shifted Gegenbauer polynomials. These new polynomials are used to define a novel set of orthogonal fractional-order shifted Gegenbauer moments (FrSGMs). The proposed method is applied in gray-scale image analysis and recognition. The invariances to rotation, scaling and translation (RST), are achieved using invariant fractional-order geometric moments. Experiments are conducted to evaluate the proposed FrSGMs and compare with the classical orthogonal integer-order Gegenbauer moments (GMs) and the existing orthogonal fractional-order moments. The new FrSGMs outperformed GMs and the existing orthogonal fractional-order moments in terms of image recognition and reconstruction, RST invariance, and robustness to noise.

Introduction

Orthogonal moments are widely used to represent signals and images [1]. The orthogonal moments are divided into two main

Peer review under responsibility of Cairo University.
* Corresponding author.
E-mail address: k_hosny@yahoo.com (K.M. Hosny).

https://doi.org/10.1016/j.jare.2020.05.024
2090-1232/

groups according to their coordinate systems, cartesian and polar coordinates. Legendre moments [2], Gegenbauer moments [3], and Gaussian-Hermite moments [4] are the most common orthogonal moments which defined in the cartesian coordinates. Zernike moments [5], pseudo-Zernike moments [6], radial harmonic Fourier moments [7], and radial substituted Chebyshev moments [8,9] are examples of circular orthogonal moments in polar coordinates.

Since, the digital images are generally defined using cartesian pixels; therefore, the use of orthogonal moments is preferable where no need for cartesian to polar image mapping. Abramowiz and Stegun, [10] showed that Gegenbauer polynomials are generic polynomials where the orthogonal polynomials of Legendre, Chebyshev of the first kind and Chebyshev of the second kind are special cases from Gegenbauer polynomials with $\alpha = 0.5$, $\alpha = 0$ and $\alpha = 1$, respectively.

Pawlak [11] showed that the scaling parameter, $\alpha > -0.5$, of the Gegenbauer polynomials is very useful in digital image processing, where an improved image reconstruction can be achieved by selecting the proper value of this scaling factor. Moreover, the adjustable scaling parameter is used to control the relation between the global and local image features where large values results in local image representation while small values results in global image features.

Hosny [3] proved that orthogonal Gegenbauer moments are able to reconstruct digital gray-scale images with minimum reconstruction error and robust to different noise. Based on these characteristics, orthogonal Gegenbauer moments were used in object recognition [12], character recognition [13], pattern recognition [14], full-field strain and displacement measurements [15,16], optics applications [17], SAR image classification [18,19], and Galaxies images classification [20].

Based on the extensive studies in the fractional calculus, mathematicians concluded that non-integer order polynomials have better abilities to represent image functions than the corresponding integer-order polynomials [21]. This conclusion motives the scientists to derive different sets of non-integer order polynomials and utilize these polynomials and their moments/coefficients to represent digital images. Xiao et al. [22] derived the fractional-order Legendre moments (FrLMs). Zhang et al. [23] derived the fractional-order Fourier-Mellin moments (FrFMMs). Benouini et al. [24] derived the fractional-order Chebyshev moments (FrCMs).

The attractive characteristics of orthogonal Gegenbauer polynomials stimulate defining orthogonal fractional-order Gegenbauer polynomials and deriving their moments. The RST invariances for these new fractional-order Gegenbauer moments are derived through the fractional-order geometric moments. The contribution of this paper is summarized as follows:

1. A new set of fractional-order shifted Gegenbauer polynomials (FrSGPs) is defined in the interval $0 \le x \le 1$.
2. New orthogonal fractional-order shifted Gegenbauer moments (FrSGMs) for gray-scale images are derived on the interval $[0 \le x \le 1] \times [0 \le y \le 1]$.
3. No need for any kind of image mapping, since both the shifted Gegenbauer polynomials and the digital images are defined in the same cartesian domain, $[0, 1] \times [0, 1]$.
4. The moment invariants to rotation, scaling and translation are derived using the fractional-order geometric moment invariants.
5. The new FrSGMs are robust to different kinds of images.

The remaining of this paper is: Preliminaries of classical integer-order Gegenbauer polynomials and their moments are presented in Section 'Preliminaries'. The derivation of the new fractional-order shifted Gegenbauer polynomials and their fractional-order moments are presented in Section 'The proposed fractional-order gegenbauer moments'. Detailed experimental work is presented in Sections 'The proposed fractional-order gegenbauer moments'. Finally, the paper is concluded in Section 'Experiments, results and discussion'.

Preliminaries

The classical integer-order Gegenbauer polynomials and the GMs for gray-scale images are briefly described.

Classical orthogonal Gegenbauer polynomials

The classical Gegenbauer polynomials of integer-order, $G_p^{(\alpha)}(x)$, is [10]:

$$G_p^{(\alpha)}(x) = \sum_{k=0}^{\lfloor \frac{p}{2} \rfloor} B_{p,k}^{(\alpha)} x^{p-2k} \tag{1}$$

where

$$B_{p,k}^{(\alpha)} = (-1)^k \frac{\Gamma(p-k+\alpha)2^{p-2k}}{k!(p-2k)!\Gamma(\alpha)} \tag{2}$$

These polynomials, $G_p^{(\alpha)}(x)$, satisfy the condition:

$$\int_{-1}^{1} G_p^{(\alpha)}(x) G_q^{(\alpha)}(x) w^{(\alpha)}(x) dx = C_p(\alpha)\delta_{pq} \tag{3}$$

where the mathematical symbols, $\Gamma(\cdot)$ & δ_{pq}, refer to the gamma and the Kronecker functions respectively; the controlling parameter, α, is a real number ($-1.5 \le \alpha$). The weight function, $w^{(\alpha)}(x)$, and the normalization constant, $C_p(\alpha)$, is defined as:

$$w^{(\alpha)}(x) = \left(1 - x^2\right)^{\alpha - 0.5} \tag{4}$$

$$C_p(\alpha) = \frac{2\pi\Gamma(p+2\alpha)}{2^{2\alpha}p!(p+\alpha)![\Gamma(\alpha)]^2} \tag{5}$$

The $G_p^{(\alpha)}(x)$ are computed using the three-term recurrence relation:

$$G_{p+1}^{(\alpha)}(x) = \frac{(2p+\alpha)}{(p+\alpha)} x G_p^{(\alpha)}(x) - \frac{(p+2\alpha-1)}{(p+1)} G_{p-1}^{(\alpha)}(x), \tag{6}$$

with $G_0^{(\alpha)}(x) = 1$, and $G_1^{(\alpha)}(x) = 2\alpha x$.

Integer-order Gegenbauer moments

The integer-order GMs of order $(p, q)$are [3]:

$$A_{pq} = \frac{1}{C_p(\alpha)C_q(\alpha)} \int_{-1}^{-1} \int_{-1}^{1} f(x,y) G_p^{(\alpha)}(x) G_q^{(\alpha)}(y) w^{(\alpha)}(x) w^{(\alpha)}(y) dxdy, \tag{7}$$

where the indices, p & q, are non-negative integers.

Since $G_p^{(\alpha)}(x)$ are orthogonal over the square $[-1, 1] \times [-1, 1]$, the image function, $f(x, y)$, of the original input images must mapped over the square $[-1, 1] \times [-1, 1]$. Theoretically, digital images could be reconstructed using an infinite number of GMs using the form:

$$f(x,y) = \sum_{p=0}^{\infty} \sum_{q=0}^{\infty} A_{pq} G_p^{(\alpha)}(x) G_q^{(\alpha)}(y) \tag{8}$$

In practice, finite summation is permitted in all computing platforms and environments, therefore, only Eq. (8) is adapted as follows:

$$\widehat{f}_{Max}(x,y)=\sum_{p=0}^{Max}\sum_{q=0}^{Max}A_{p,q}G_p^{(\alpha)}(x)G_q^{(\alpha)}(y), \tag{9}$$

The value of*Max* is defined by the user and the total number of extracted features are:

$$N_{Total}=(Max+1)^2 \tag{10}$$

The proposed fractional-order Gegenbauer moments

This section presents a description of the proposed fractional-order Gegenbauer Moments. Novel fractional-order shifted Gegenbauer polynomials are derived. Then, the new FrSGMs for gray-scale images derived. The mathematical derivation of RST invariances is presented. Finally, the numerical integration method for accurate and efficient computation of FrSGMs is described.

Orthogonal fractional-order shifted Gegenbauer polynomials

Assume λ is a real number ($\lambda>0$). The fractional-order shifted Gegenbauer polynomials,$FrG_p^{(\alpha)}(t)$, are derived by replacing the variable $x=2t^{\lambda}-1$ with $t\in[0,1]$ in Eq. (1). Then, $FrG_p^{(\alpha)}(t)$ are defined as:

$$FrG_p^{(\alpha)}(t)=G_p^{(\alpha)}\left(2t^{\lambda}-1\right), \tag{11}$$

The explicit form of the fractional-order shifted Gegenbauer polynomials, $FrG_p^{(\alpha)}(t)$, of degree p is:

$$FrG_p^{(\alpha)}(t)=\sum_{k=0}^{\lfloor\frac{p}{2}\rfloor}B_{p,k}^{(\alpha)}\left(2t^{\lambda}-1\right)^{p-2k}, \tag{12}$$

The Fractional-order shifted Gegenbauer polynomials,$FrG_p^{(\alpha)}(t)$, are obeying the following recurrence relation:

$$FrG_{p+1}^{(\alpha)}(t)=\frac{(2p+\alpha)}{(p+\alpha)}\left(2t^{\lambda}-1\right)FrG_p^{(\alpha)}(t)-\frac{(p+2\alpha-1)}{(p+1)}FrG_{p-1}^{(\alpha)}(t), \tag{13}$$

with$FrG_0^{(\alpha)}(t)=1$, and $FrG_1^{(\alpha)}(t)=2\alpha\left(2t^{\lambda}-1\right)$.

The fractional-order shifted Gegenbauer polynomials, $FrG_p^{(\alpha)}(t)$, are orthogonal over the square $[0,1]\times[0,1]$, where:

$$\int_0^1 FrG_p^{(\alpha)}(t)FrG_q^{(\alpha)}(t)w^{*(\alpha)}(t)dt=C_p^*(\alpha)=\frac{1}{2\lambda}C_p(\alpha)\delta_{pq} \tag{14}$$

The modified weight function, $w^{*(\alpha)}(t)$, and the modified normalization constant, $C_p^*(\alpha)$, are defined as:

$$w^{*(\alpha)}(t)=t^{\lambda-1}\left(4t^{\lambda}-4t^{2\lambda}\right)^{\alpha-0.5}$$

$$C_p^*(\alpha)=\frac{2\pi\Gamma(p+2\alpha)}{\lambda 2^{2\alpha+1}p!(p+\alpha)![\Gamma(\alpha)]^2}. \tag{15}$$

Proof of orthogonality property:

Proof. Assume $x=2t^{\lambda}-1$, then $dx=2\lambda t^{\lambda-1}dt$, substituting these values in Eq. (3) yields:

$$\begin{aligned}
&\int_0^1 G_p^{(\alpha)}\left(2t^{\lambda}-1\right)G_q^{(\alpha)}\left(2t^{\lambda}-1\right)w^{(\alpha)}\left(2t^{\lambda}-1\right)2\lambda t^{\lambda-1}dt=C_p(\alpha)\delta_{pq}\\
&=\int_0^1 FrG_p^{(\alpha)}(t)FrG_q^{(\alpha)}(t)\left(4t^{\lambda}-4t^{2\lambda}\right)^{\alpha-0.5}2\lambda t^{\lambda-1}dt=C_p(\alpha)\delta_{pq}\\
&=2\lambda\int_0^1 FrG_p^{(\alpha)}(t)FrG_q^{(\alpha)}(t)\left(4t^{\lambda}-4t^{2\lambda}\right)^{\alpha-0.5}t^{\lambda-1}dt=C_p(\alpha)\delta_{pq}\\
&=2\lambda\int_0^1 FrG_p^{(\alpha)}(t)FrG_q^{(\alpha)}(t)w^{*(\alpha)}(t)dt=C_p(\alpha)\delta_{pq}\\
&=\int_0^1 FrG_p^{(\alpha)}(t)FrG_q^{(\alpha)}(t)w^{*(\alpha)}(t)dt=\frac{1}{2\lambda}C_p(\alpha)\delta_{pq}=C_p^*(\alpha)\delta_{pq}
\end{aligned}$$

Fractional-order shifted Gegenbauer moments for gray-scale images

The FrSGMs of order $(p,q)$are:

$$FrA_{pq}=\frac{1}{C_p^*(\alpha)C_q^*(\alpha)}\int_0^1\int_0^1 f(x,y)FrG_p^{(\alpha)}(x)FrG_q^{(\alpha)}(y)w^{*(\alpha)}(x)w^{*(\alpha)}(y)dxdy \tag{16}$$

where the functions, $FrG_p^{(\alpha)}(x)$, are the real-valued fractional order Gegenbauer polynomial of the pth order.

Digital images could be reconstructed using $FrG_p^{(\alpha)}(x)$ and FrSGMs in the square cartesian domain $[0,1]\times[0,1]$:

$$f(x,y)=\sum_{p=0}^{\infty}\sum_{q=0}^{\infty}FrA_{pq}FrG_p^{(\alpha)}(x)FrG_q^{(\alpha)}(y) \tag{17}$$

Or in approximate form based on *Max* as follows:

$$\widehat{f}_{Max}(x,y)=\sum_{p=0}^{Max}\sum_{q=0}^{Max}FrA_{p,q}\mathrm{FrG}_p^{(\alpha)}(x)\mathrm{FrG}_q^{(\alpha)}(y), \tag{18}$$

where the total number of moments to be used for image generation is defined as in Eq. (10).

Fractional-order shifted Gegenbauer moment invariants

Fractional-order geometric moments

The fractional-order geometric Moments (FrGMs) of order $\lambda(p+q)$ for the image function, $f(x_i,y_j)$, with size, $N\times N$, are [22,24]:

$$GM_{pq}^{\lambda}=\sum_{i=1}^{N}\sum_{j=1}^{N}f(x_i,y_j)m_{pq}(x_i,y_j), \tag{19}$$

$$m_{pq}(x_i,y_j)=\int_{x_i-\frac{\Delta x}{2}}^{x_i+\frac{\Delta x}{2}}\int_{y_j-\frac{\Delta y}{2}}^{y_j+\frac{\Delta y}{2}}x^{\lambda p}y^{\lambda q}dxdy \tag{20}$$

with $\lambda\in R^{+}$.

The image centroid, $(\hat{x},\hat{y})\in[0,1]$, is:

$$\hat{x}=\frac{GM_{10}^{\lambda}}{GM_{00}^{\lambda}},\quad \hat{y}=\frac{GM_{01}^{\lambda}}{GM_{00}^{\lambda}}\quad \text{with}\ \ \lambda=1 \tag{21}$$

Let λ has an odd denominator and can be written as $\frac{2b}{2a+1}$ with $a,b\in n$, where $a\neq0$. The translation invariant fractional-order central moments are:

$$Z_{pq}^{\lambda}=\sum_{i=1}^{N}\sum_{j=1}^{N}f(\mathrm{x_i},y_j)z_{pq}(\mathrm{x_i},y_j) \tag{22}$$

where

$$z_{pq}(x_i,y_j)=\int_{x_i-\frac{\Delta x}{2}}^{x_i+\frac{\Delta x}{2}}\int_{y_j-\frac{\Delta y}{2}}^{y_j+\frac{\Delta y}{2}}(x-\widehat{x})^{\lambda p}(y-\widehat{y})^{\lambda q}dxdy \tag{23}$$

with λ should satisfy the odd denominator condition.

The fractional-order geometric moment invariants, G_{pq}^{λ}, could be expressed as:

$$G_{pq}^{\lambda}=\beta^{-\gamma}\sum_{i=1}^{N}\sum_{j=1}^{N}f(x_i,y_j)v_{pq}(x_i,y_j) \tag{24}$$

where

$$v_{pq}(\mathrm{x_i},\mathrm{y_j})=\int_{x_i-\frac{\Delta x}{2}}^{x_i+\frac{\Delta x}{2}}\int_{y_j-\frac{\Delta y}{2}}^{y_j+\frac{\Delta y}{2}}\Big\{\big[(\mathrm{x}-\widehat{\mathrm{x}})\cos\theta+(\mathrm{y}-\widehat{\mathrm{y}})\sin\theta\big]^{\lambda \mathrm{p}}\big[(\mathrm{y}-\widehat{\mathrm{y}})\cos\theta-(\mathrm{x}-\widehat{\mathrm{x}})\sin\theta\big]^{\lambda \mathrm{q}}\Big\}\mathrm{dxdy} \tag{25}$$

The normalization parameters β, γ and θ, are defined in [24]. For $\lambda=1$, these parameters could be determined as follows:

$$\lambda=GM_{00}^{\lambda},\quad \gamma=\frac{\lambda(\mathrm{p}+\mathrm{q})+2}{2}\ \text{ and }\ \theta=\frac{1}{2}\tan^{-1}\left(\frac{2Z_{11}^{\lambda}}{Z_{20}^{\lambda}-Z_{02}^{\lambda}}\right) \tag{26}$$

Fractional-order shifted Gegenbauer moment invariants

This subsection studies the invariants of FrSGMs to the geometric transformations, RST. Using the relation between the FrSGPs and the geometric basis $\{x^{\lambda p}y^{\lambda q}\}$. The FrSGMs can be expressed in terms of GM_{pq}^{λ}. Therefore, Eq. (16) can be reformulated as follows:

$$FrA_{pq}=\frac{1}{C_p^*(\alpha)C_q^*(\alpha)}\sum_{k=0}^{\mathrm{p}}\sum_{l=0}^{\mathrm{q}}B_{p,k}^{(\alpha)}B_{q,l}^{(\alpha)}w^{*(\alpha)}(x)w^{*(\alpha)}(y)GM_{pq}^{\lambda} \tag{27}$$

By replacing the GM_{pq}^{λ} in the Eq. (27) by G_{pq}^{λ} of Eq. (24), the RST invariants of FrSGMs, which called FrSGMIs are:

$$FrSGMI_{pq}=\frac{1}{C_p^*(\alpha)C_q^*(\alpha)}\sum_{k=0}^{\mathrm{p}}\sum_{l=0}^{\mathrm{q}}B_{p,k}^{(\alpha)}B_{q,l}^{(\alpha)}w^{*(\alpha)}(x)w^{*(\alpha)}(y)G_{pq}^{\lambda} \tag{28}$$

with the condition that λ has odd denominators.

Accurate computation of the FrSGMs

In this section, the authors describe how the FrSGMs are computed using the accurate Gaussian quadrature numerical integration methodology [25]. For gray-scale image $f(x,y)$ of size $N\times N$, an image intensity function $f(i,j)$ defined on a discrete domain , where $i=1,2,3,\ldots,N$, and $j=1,2,3,\ldots,N$. The image is mapped to a domain of $(x_i,y_j)\in[0,1]\times[0,1]$. Therefore, the points of mapped image coordinates $(\mathrm{x_i},\mathrm{y_j})$ are defined as:

$$x_i=\frac{i}{N}+\frac{\Delta x}{2}, \tag{29}$$

$$\mathrm{y_j}=\frac{j}{N}+\frac{\Delta y}{2} \tag{30}$$

with $\Delta x=1/N$ and $\Delta y=1/N$.

Inspired by the kernel-based approach for efficient computation of orthogonal moments [26], the FrSGMs as given by Eq. (16) are reformulated:

$$FrA_{pq}(f)=\frac{1}{C_p^*(\alpha)C_q^*(\alpha)}\sum_{i=1}^{N}\sum_{j=1}^{N}T_{pq}(x_i,y_j)f(x_i,y_j) \tag{31}$$

where

$$T_{pq}(x_i,y_j)=\int_{x_i-\frac{\Delta x}{2}}^{x_i+\frac{\Delta x}{2}}\int_{y_j-\frac{\Delta y}{2}}^{y_j+\frac{\Delta y}{2}}FrG_p^{(\alpha)}(x)FrG_q^{(\alpha)}(y)w^{*(\alpha)}(x)w^{*(\alpha)}(y)dxdy \tag{32}$$

Eq. (32) could be expressed using both x-and y-kernels as follows:

$$FrA_{pq}(f)=\frac{1}{C_p^*(\alpha)C_q^*(\alpha)}\sum_{i=1}^{N}\sum_{j=1}^{N}IX_p(x_i)IY_q(y_j)f(x_i,y_j) \tag{33}$$

where

$$IX_p(x_i)=\int_{x_i-\frac{\Delta x}{2}}^{x_i+\frac{\Delta x}{2}}FG_p^{(\alpha)}(x)w^{*(\alpha)}(x)dx \tag{34}$$

$$IY_q(y_j)=\int_{y_j-\frac{\Delta y}{2}}^{y_j+\frac{\Delta y}{2}}FG_q^{(\alpha)}(y)w^{*(\alpha)}(y)dy \tag{35}$$

For simplicity, the limits of the definite integrals are:

$$U_{i+1}=x_i+\frac{\Delta x}{2},\quad \mathrm{U_i}=\mathrm{x_i}-\frac{\Delta x}{2} \tag{36}$$

$$V_{j+1}=y_j+\frac{\Delta y}{2},\quad \mathrm{V_j}=y_j-\frac{\Delta y}{2} \tag{37}$$

Eqs. (34) and (35) can be expressed as follows:

$$IX_p(x_i)=\int_{U_i}^{U_{i+1}}FrG_p^{(\alpha)}(x)w^{*(\alpha)}(x)dx=\int_{U_i}^{U_{i+1}}RX(x)dx \tag{38}$$

$$IY_q(y_j)=\int_{V_j}^{V_{j+1}}FrG_q^{(\alpha)}(y)w^{*(\alpha)}(y)dy=\int_{V_j}^{V_{j+1}}RY(y)dy \tag{39}$$

where $RX(x)=FG_p^{(\alpha)}(x)w^{*(\alpha)}(x)$ and $RY(y)=FG_q^{(\alpha)}(y)w^{*(\alpha)}(y)$

Since, the analytical evaluation of the finite integrals of the kernels, $IX_p(x_i)$ and $IY_q(y_j)$, as defined in Eqs. (38) and (39) is impossible, Therefore, the kernels, $IX_p(x_i)$and $IY_q(y_j)$, are computed by the accurate Gaussian quadrature [25] approximation. The definite integral, $\int_a^b h(z)dz$, could be computed as:

$$\int_a^b h(z)dz\approx\frac{(b-a)}{2}\sum_{l=0}^{c-1}w_l h\left(\frac{a+b}{2},\frac{b-a}{2}t_l\right) \tag{40}$$

where the detailed implementation of this method could be found in [27,28].

Substituting equation (40) into (38) yields:

$$IX_p(x_i)=\int_{U_i}^{U_{i+1}}RX(x)dx\approx\frac{(U_{i+1}-U_i)}{2}\sum_{l=0}^{c-1}w_l RX\left(\frac{U_{i+1}+U_i}{2}+\frac{U_{i+1}-U_i}{2}t_l\right) \tag{41}$$

Similarly:

$$IY_q(y_j) = \int_{U_i}^{U_{i+1}} RY(y)dy \approx \frac{(V_{j+1}-V_j)}{2}\sum_{l=0}^{c-1} w_l RY\left(\frac{V_{j+1}+V_j}{2}+\frac{V_{j+1}-V_j}{2}t_l\right) \quad (42)$$

Direct calculation of FrSGMs using Eq. (33) is time-consuming task where heavy computational-costs of $C_p^*(\alpha)$ which required computing factorials and Gamma functions for each moment order. The computational complexity of this equation could be reduced by using the recurrence form.

$$C_p^*(\alpha) = \frac{(p-1+\alpha)(p-1+2\alpha)}{p(p+\alpha)} C_{p-1}^*(\alpha), \quad (43)$$

with

$$C_0^*(\alpha) = \frac{2\pi\Gamma(2\alpha)}{\lambda 2^{2\alpha+1}\alpha[\Gamma(\alpha)]^2}. \quad (44)$$

Similarly, another recurrence relation is employed to compute $FrG_p^{(\alpha)}(x)$ and $FrG_p^{(\alpha)}(y)$for fast computation of $IX_p(x_i)$ and $IY_q(y_j)$. Moreover, the successful 1-D moment computation [3] is employed:

$$FrA_{pq} = \sum_{i=1}^{N} IX_p(x_i) Y_{iq}, \quad (45)$$

where

$$Y_{iq} = \sum_{j=1}^{N} IY_q(y_j) f(x_i, y_j), \quad (46)$$

Experiments, results and discussion

This section presented the performed numerical experiments, the obtained results and the discussion. Four experiments were conducted to assess FrSGMs and compare its performance with GMs [3] and the existing fractional-order moments such as FrLFMs [22], FrFMMs [23] and FrCMs [24]. One experiment is performed where a standard gray-scale image is reconstructed. This experiment is used to assess the accuracy. The invariances to similarity transformations, RST, of the proposed moments is tested in the second group. Sensitivity to noise is assessed in the third experiment. Finally, image recognition is quantitively measured in the fourth experiment.

Image reconstruction

Image reconstruction using orthogonal moments is an essential process in different image processing applications. This process used to measure accuracy and numerical stability of the computed moments. The reconstructed images are evaluated using the normalized image reconstruction error (NIRE) [29] which is a quantative measure:

$$NIRE = \frac{\sum_{i=0}^{N-1}\sum_{j=0}^{N-1}\left(f(i,j) - f^{Recontructed}(i,j)\right)^2}{\sum_{i=0}^{N-1}\sum_{j=0}^{N-1}(f(i,j))^2} \quad (47)$$

Continues decreasing of NIRE values reflects accuracy and stability of the computed moments.

The proposed fractional-order shifted Gegenbauer moments, FrSGMs, and the orthogonal moments [3,22–24] used in reconstructing the standard gray-scale image, "peppers", using low and high orders, 15, 25, 35, 45, 60, 80, 100, 150 & 200, with $\alpha = 1.2$, where Fig. 1 shows the values of the quantative measure. The reconstructed images with the corresponding NIRE values are displayed in Fig. 2.

Figs. 1 and 2 show that the FrOFMMs [23] is not able to reconstruct gray-scale images. For low order, $max \leq 40$, the integer-order GMs [3] and the FrLFMs [22] can reconstruct gray-scale images with moderate quality. On the other side, the proposed moments, FrSGMs, and the FrCMs can reconstruct gray-scale images for both low and higher-order moments.

Both FrSGMs and FrCMs show the similar ability for low orders while for higher orders, the proposed FrSGMs outperformed all other existing methods. These results ensure the accuracy and stability of the proposed method.

Invariance to RST

Invariances to RST, are essential characteristics for pattern recognition and computer vision applications. Each invariance is

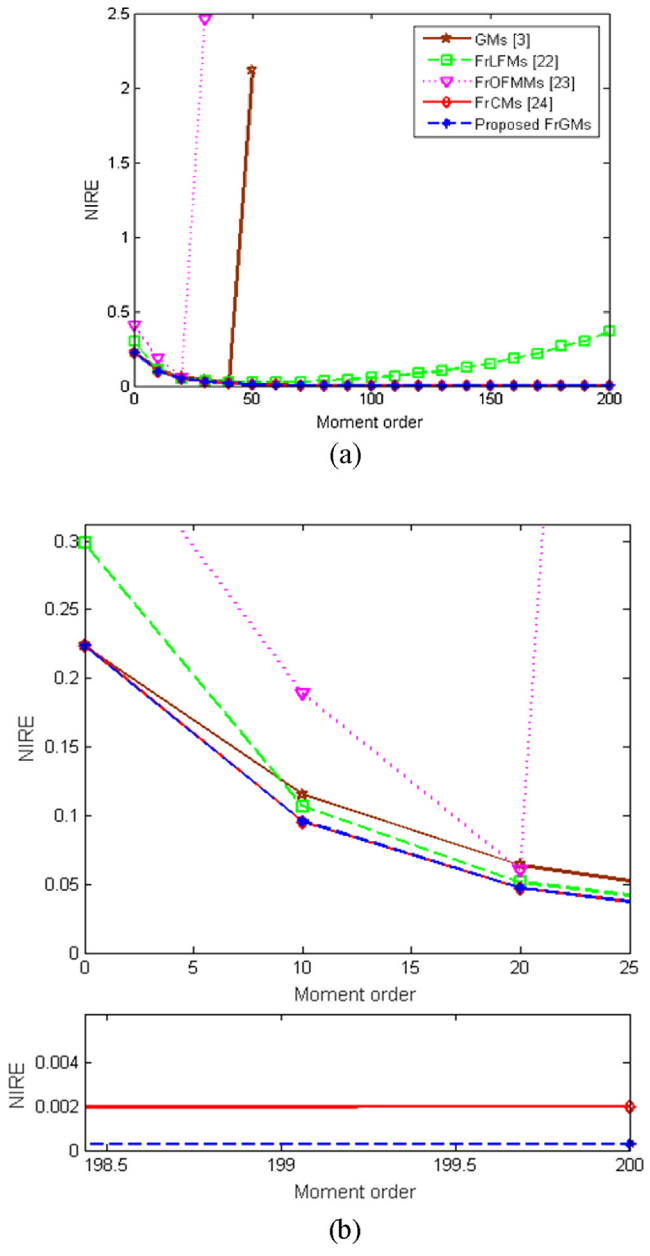

Fig. 1. The NIRE values of FrSGMs, the orthogonal moments [3,22–24], for the Peppers' image of size 128 × 128, (a): The original curves, (b): Zoom-in-curves.

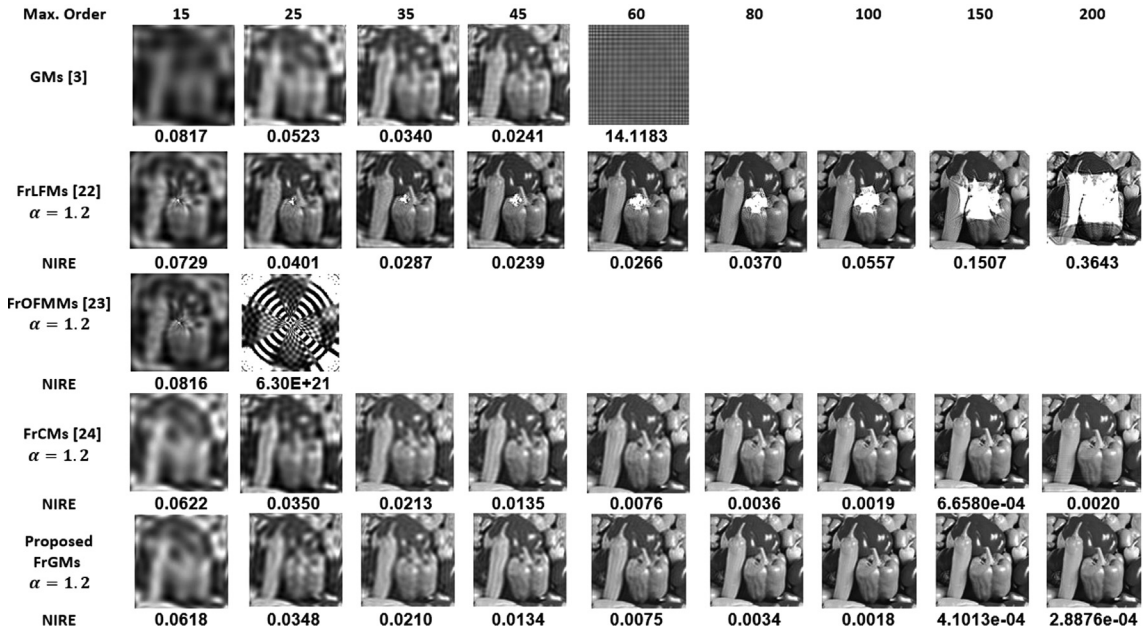

Fig. 2. The reconstructed images using the proposed FrSGMs and the orthogonal moments [3,22–24].

assessed by an individual experiment, where these invariances could be evaluated using the following quantitative measure.

$$MSE = \frac{1}{L_{Total}} \sum_{p=0}^{Max} \sum_{q=0}^{Max} \left(|FrA_{pq}(f)| - |FrA_{pq}\left(f^{Trans.}\right)| \right)^2 \quad (48)$$

where L_{total} is an integer refers to the total number of the independent moments; the terms $|FrA_{pq}\left(f^{Trans.}\right)|$ and $|FrA_{pq}(f)|$ are the values of the magnitudes of the utilized moments for both transformed and original images.

First experiment: the gray-scale image of "Lena" with size 256×256 is rotated by different angles from 0° to 90° in the counter-clockwise direction. The proposed FrSGMs, GMs [3], FrLFMs [22], FrOFMMs [23] and FrCMs [24] are calculated for each image, original & rotated, using maximum moment order equal to 20. The MSE for the five groups of orthogonal moments where evaluated where the plotted curves are displayed in Fig. 3.

The plotted curves in Fig. 3 show that the MSE values of FrLFMs [22] and FrOFMMs [23] are high, which reflects their lousy performance. The existing methods, GMs [3] and FrCMs [24] have relatively small MSE values, which indicate good rotation invariance. On the other side, the proposed FrSGMs have the lowest values of MSE and the best rotation invariance performance.

Second experiment: the well-known COIL-20 dataset [30] is used in this experiment. The gray-scale image of the object obj4_0 of size 128×128 is scaled using 3 reduction scaling factors, 0.25, 0.5, & 0.75; and 4 magnification scaling factors,1.25, 1.5, 1.75, & 2.0. The proposed FrSGMs, GMs [3], FrLFMs [22], FrOFMMs [23] and FrCMs [24] are calculated for original, reduced and magnified images of the selected object using maximum moment order equal to 20. Fig. 4(a and b) shows the MSE values for reduced and magnified images. The proposed FrSGMs results in the smallest values of MSE.

Third experiment: the gray-scale image of the object obj3_0 [30] is translated using various translation parameters in horizontal and vertical directions. The proposed FrSGMs and the orthogonal moments [3,22–24] are calculated where Fig. 5 shows the MSE for all moments.

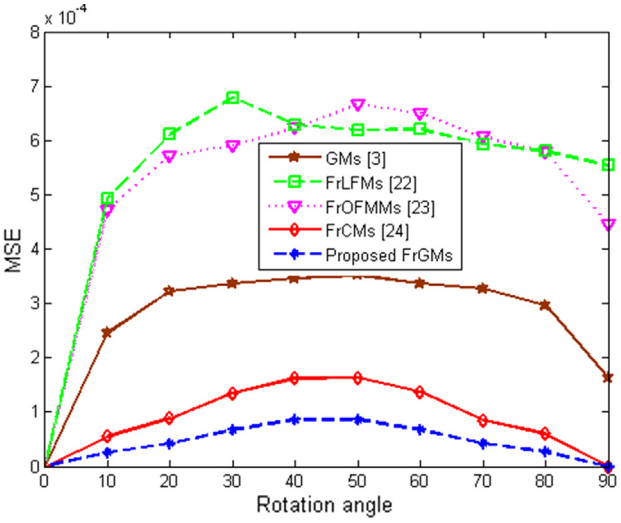

Fig. 3. The MSE values for rotation angles using the proposed FrSGMs and the orthogonal moments [3,22–24].

Again, the proposed orthogonal FrSGMs show small MSE values which ensure the highly accurate invariances to the RST geometric transformations. These new fractional-order moments outperformed the integer-order orthogonal moments [3] and the existing fractional-order moment [22–24].

Robustness against noise

In this subsection, three experiments were performed to test the sensitivity of the proposed FrSGMs to noise. Different levels of 'salt & peppers', white Gaussian, and speckle noise are added to the standard gray-scale image of the object obj17_0 [30] where Fig. 6 shows the standard and contaminated images.

MSE values are computed using the proposed FrSGMs and the orthogonal moments [3,22–24] for contaminated images and displayed in Fig. 6(b–d). FrSGMs are less sensitive to noise than the integer-order Gegenbauer moments, GMs [3] and the existing

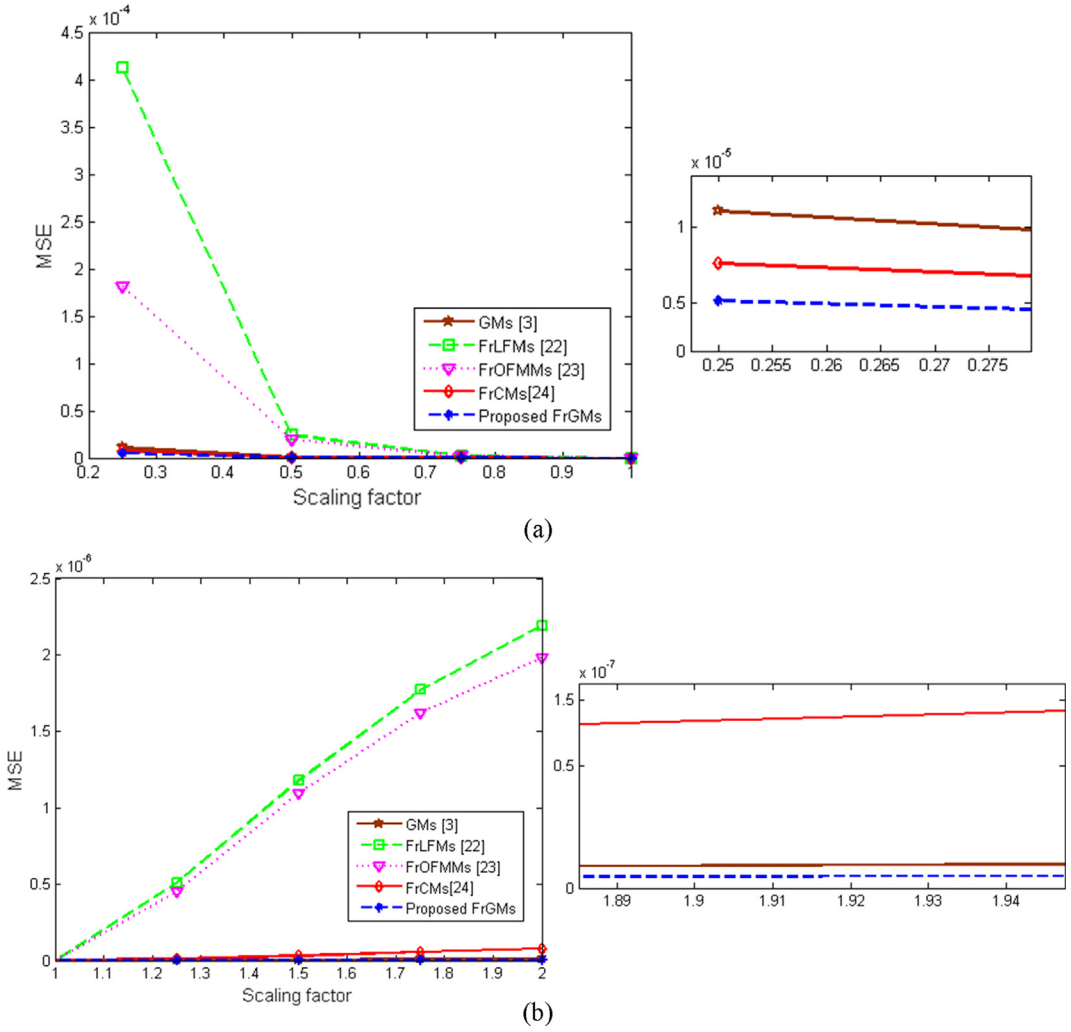

Fig. 4. The MSE values for scaling invariance using the proposed FrSGMs and the orthogonal moments [3,22–24]: (a) Reduction, (b) Magnification.

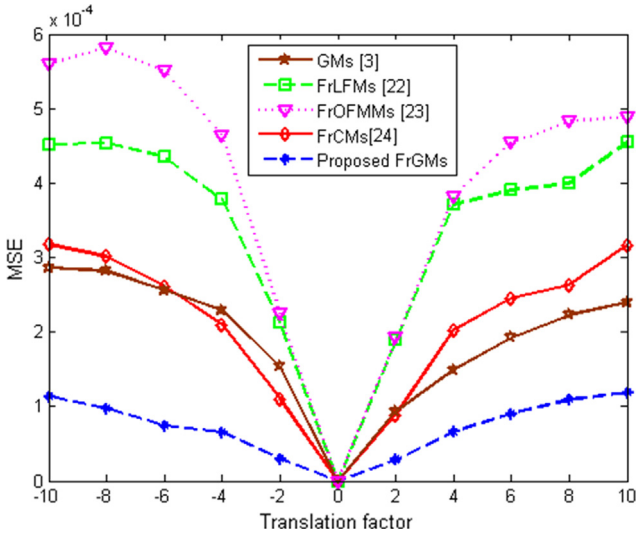

Fig. 5. MSE for the translated images calculated by using the proposed FrSGMs and the orthogonal moments [3,22–24].

fractional-order moments, FrLFMs [22], FrOFMMs [23] and FrCMs [24].

Image recognition

In this subsection, the recognition ability of the proposed FrSGMs moments is evaluated using the well-known dataset of birds [31]. This dataset is consisting of six classes with 100 different size images in each class. For simplicity, images are resized to a unified size 512×512.

The recognition rate, RT(%) [9] is used to quantitively measure the ability of the proposed FrSGMs moments to recognize the similar gray-scale images. It is defined as:

$$RT(\%) = \frac{(Y \times 100)}{Qr} \tag{49}$$

where Qr and Y refers to query and correctly identified images. To avoid any biased results, 5 distance similarity measures, L_1-norm, L_2-norm, square-chord, χ^2, and Canberra are used in computing RT(%).

The proposed FrSGMs, and the orthogonal moments [3,22–24] were computed in 4 experiments. The first experiment is called "normal" where all images are not subjected to any kind of transformations and noise-free. The second experiment is called "rotation" where all images are rotated. In the third and the fourth experiments, all images are scaled and contaminated with noise.

In the performed experiments, the maximum moment' orders were selected to unified the length of feature vectors. The

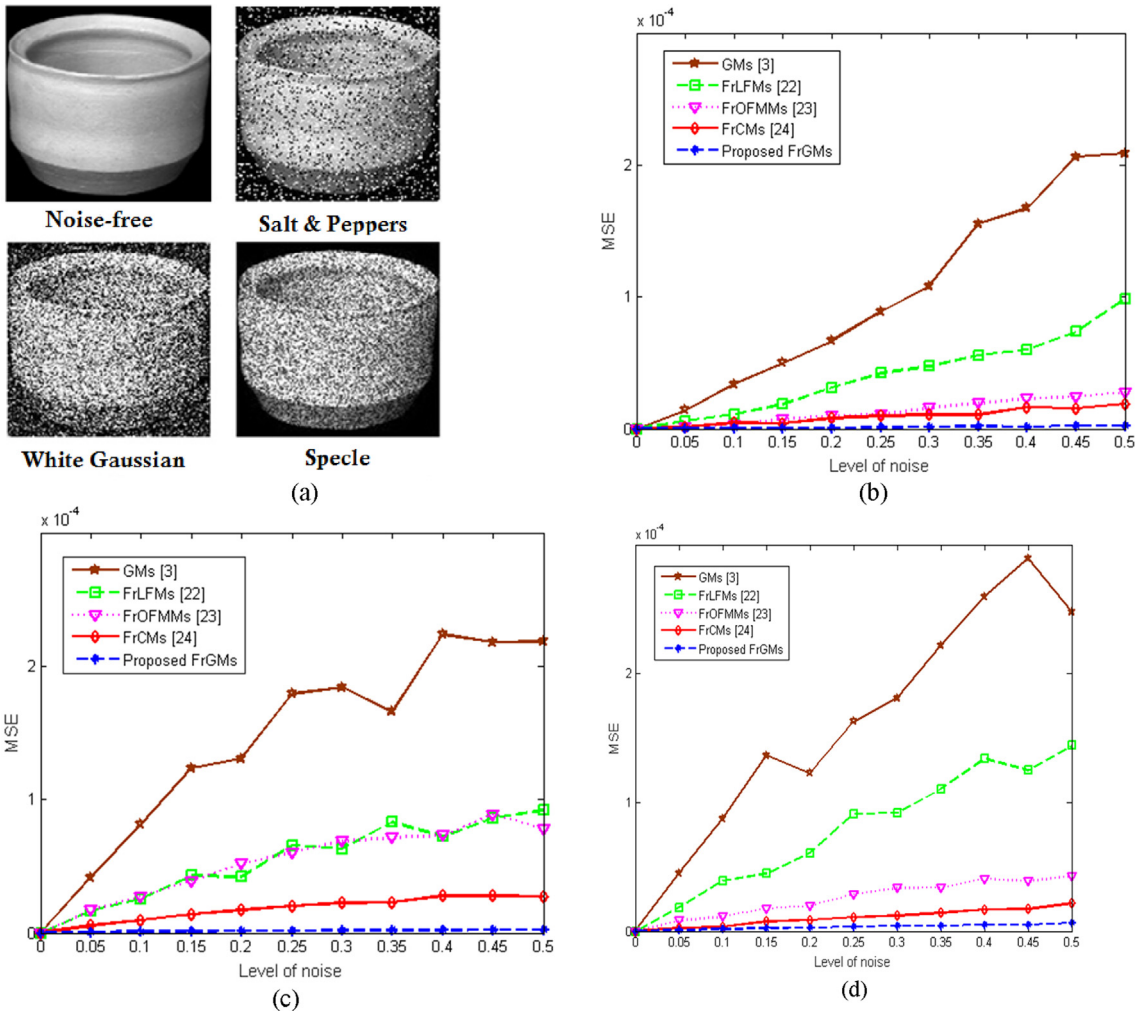

Fig. 6. MSE values of the noisy grayscale images of obj17_0 [30] for FrSGMs and the existing methods [3,22–24]: (a) Noise-free image, and contaminated images using "salt & peppers", white Gaussian, and speckle (b) Salt & Peppers, (c) white Gaussian, (d) Speckle.

maximum value, Max = 5, is used with the FrLFMs [22], FrOFMMs [23] which results in 66 features. Finally, the maximum value, *Max* = 7, is used for the proposed FrSGMs and FrCMs [24], which results in 64 features.

Table 1
Recognition rates *R* (%) of (|FrSGMs|), and the orthogonal moments [3,22–24] for the normal dataset of Bird, with $\alpha = 1.2$.

Similarity measure	Methods				
	GMs [3]	FrLFMs [22]	FrOFMMs [23]	FrCHMs [24]	Proposed FrSGMs
*L*1-norm	68.43	55.39	45.94	72.56	75.57
*L*2-norm	70.78	57.15	47.41	74.68	77.60
Square-chord	68.49	53.35	42.24	72.38	74.66
$\chi 2$	69.41	54.76	42.86	73.55	76.37
Canberra	67.35	52.81	38.53	71.28	73.69
Mean recognition rate	68.89	54.69	43.40	72.89	75.58

Table 2
Recognition rates *R* (%) of (|FrSGMs|), and the orthogonal moments [3,22–24] for the randomly rotated dataset of Birds, with $\alpha = 1.2$.

Similarity measure	Methods				
	GMs [3]	FrLFMs [22]	FrOFMMs [23]	FrCMs [24]	Proposed FrSGMs
*L*1-norm	69.85	55.91	47.15	74.21	76.15
*L*2-norm	71.59	57.53	48.23	75.75	77.98
Square-chord	67.75	54.24	43.37	72.26	74.53
$\chi 2$	69.37	55.32	43.81	73.55	76.373
Canberra	67.24	53.19	39.45	71.43	73.74
Mean recognition rate	69.16	55.24	44.40	73.44	75.76

Table 3
Recognition rates R (%) (|FrSGMs|), and the orthogonal moments [3,22–24] for randomly scaled dataset of Birds, with $\alpha = 1.2$.

Similarity measure	Methods				
	GMs [3]	FrLFMs [22]	FrOFMMs [23]	FrCHMs [24]	Proposed FrSGMs
L1-norm	70.63	56.58	48.23	74.60	77.32
L2-norm	72.29	57.97	49.34	76.03	79.11
Square-chord	68.65	54.82	46.75	72.81	75.85
$\chi 2$	69.36	55.79	47.32	73.86	77.52
Canberra	67.75	53.64	40.86	71.77	74.90
Mean recognition rate	69.74	55.76	46.50	73.82	76.94

Table 4
Recognition rates R (%) of (|FrSGMs|), and the orthogonal moments [3,22–24] for the noisy dataset of Birds with $\alpha = 1.2$.

Level of noise	Similarity measure	Methods				
		GMs [3]	FrLFMs [22]	FrOFMMs [23]	FrCMs [24]	Proposed FrSGMs
Noise-free	$L1$-norm	73.15	54.03	47.56	75.56	77.89
	$L2$-norm	74.43	53.57	49.05	76.84	79.24
	Square-chord	71.19	51.10	43.69	73.60	75.82
	$\chi 2$	72.33	52.24	44.36	74.74	77.02
	Canberra	69.97	51.62	39.97	72.38	74.53
$\sigma = 0.05$	$L1$-norm	72.06	52.53	45.03	74.47	76.73
	$L2$-norm	71.94	53.94	45.33	74.35	76.61
	Square-chord	69.27	51.03	42.43	71.68	73.79
	$\chi 2$	71.20	51.65	42.72	73.61	75.83
	Canberra	69.24	50.97	39.23	71.65	73.76
$\sigma = 0.1$	$L1$-norm	71.08	50.68	43.62	73.49	75.70
	$L2$-norm	71.70	52.01	44.58	74.11	76.35
	Square-chord	68.71	49.66	42.13	71.12	73.19
	$\chi 2$	70.73	49.48	42.65	73.14	75.33
	Canberra	67.26	48.39	36.77	69.67	71.66
$\sigma = 0.15$	$L1$-norm	67.37	48.69	40.34	69.78	71.78
	$L2$-norm	69.33	49.44	41.39	71.74	73.85
	Square-chord	66.97	47.25	39.53	69.38	71.36
	$\chi 2$	68.15	49.23	39.38	70.56	72.61
	Canberra	66.02	47.69	35.28	68.43	70.36
$\sigma = 0.2$	$L1$-norm	65.79	48.33	38.26	68.20	68.28
	$L2$-norm	67.66	49.41	39.3	70.07	70.20
	Square-chord	65.60	48.04	36.47	68.01	68.08
	$\chi 2$	66.45	47.61	37.07	68.86	68.96
	Canberra	65.79	47.24	34.61	68.20	68.28
Average recognition rate	$L1$-norm	69.89	50.85	42.96	72.30	74.08
	$L2$-norm	71.01	51.67	43.93	73.42	74.87
	Square-chord	68.35	49.41	40.85	70.76	72.45
	$\chi 2$	69.77	50.04	41.24	72.18	73.95
	Canberra	67.65	49.18	37.17	70.07	71.72

The obtained results for the normal, rotated, scaled, and noisy query images are shown in the Tables 1–4, respectively. The proposed FrSGMs achieved higher recognition rates than the GMs [3], FrLFMs [22], FrOFMMs [23] and FrCMs [24].

Conclusion

Novel orthogonal fractional-order shifted Gegenbauer polynomials and moments are presented to analyze and recognize gray-scale images. The proposed fractional-order moments show excellent capabilities in image reconstruction with lower and higher moment orders, which is an essential characteristic for image processing applications. The proposed FrSGMs are insensitive to noise and invariant to RST, which improve their recognition capabilities. Based on the obtained results, the proposed FrSGMs are very useful descriptors.

Compliance with ethics requirements

All Institutional and National Guidelines for the care and use of animals (fisheries) were followed.

All procedures followed were in accordance with the ethical standards of the responsible committee on human experimentation (institutional and national) and with the Helsinki Declaration of 1975, as revised in 2008 (5). Informed consent was obtained from all patients for being included in the study.

This article does not contain any studies with human or animal subjects.

Declaration of Competing Interest

The authors declared that there is no conflict of interest.

References

[1] Flusser J, Suk T, Zitova B. 2D and 3D image analysis by moments. John Wiley & Sons; 2016 [ISBN: 9781119039372].
[2] Teague MR. Image analysis via the general theory of moments. J Opt Soc Am 1980;70(8):920–30.
[3] Hosny KM. Image representation using accurate orthogonal Gegenbauer moments. Pattern Recogn Lett 2011;32(6):795–804.
[4] Dai Bo Yang Mo. Image analysis by Gaussian-Hermite moments. Signal Process 2011;91(10):2290–303.
[5] Khotanzad A, Hong YH. Invariant image recognition by Zernike moments. IEEE Trans Pattern Anal Mach Intell 1990;12(5):489–97.

[6] Bailey RR, Srinath MD. Orthogonal moment features for use with parametric and non-parametric classifiers. IEEE Trans Pattern Anal Mach Intell 1996;18(4):389–99.
[7] Ren HP, Ping ZL, Bo WRG, Wu WK, Sheng YL. Multi-distortion-invariant image recognition with radial harmonic Fourier moments. J Opt Soc Am A 2003;20(4):631–7.
[8] Hosny KM, Darwish MM. New set of quaternion moments for color images representation and recognition. J Math Imaging Vision 2018;60(5):717–36.
[9] Hosny KM, Darwish MM. New set of multi-channel orthogonal moments for color image representation and recognition. Pattern Recogn 2019;78:376–92.
[10] Abramowiz M, Stegun IA. Hand book of mathematical functions. New York: Dover Publications; 1965.
[11] Pawlak M. Image analysis by moments: reconstruction and computational aspects. Wroclaw: Oficyna Wydawnicza Politechniki Wroc_lawskiej; 2006.
[12] Liao S, Chen J. Object recognition with lower order Gegenbauer moments. Lect Notes Softw Eng 2013;1(4).
[13] Salouan R, Safi S, Bouikhalene B. Handwritten Arabic characters recognition using methods based on Racah, Gegenbauer, Hahn, Tchebychev and orthogonal Fourier-Mellin moments. Int J Adv Sci Technol 2015;78:13–28.
[14] Hosny KM. New set of Gegenbauer moment invariants for pattern recognition applications. Arab J Sci Eng 2014;39(10):7097–107.
[15] Wang W, Mottershead JE. Adaptive moment descriptors for full-field strain and displacement measurements. J Strain Anal Eng Design 2013;48(1):16–35.
[16] Wang Weizhuo, Mottershead John E. Principles of image processing and feature recognition applied to full-field measurements. Spec Top Struct Dyn 2013;6:411–24.
[17] Wang Kejia, Ping Ziliang, Sheng Yunlong. Development of image invariant moments—a short overview. Chin Opt Lett 2016;14(9).
[18] Bolourchi P, Demirel H, Uysal S. Entropy-score-based feature selection for moment-based SAR image classification. Electron Lett 2018;54(9):593–5.
[19] Bolourchi Pouya, Moradi Masoud, Demirel Hasan, Uysal Sener. Improved SAR target recognition by selecting moment methods based on Fisher score. Signal Image Video Process (SIViP 14) 2020:39–47.
[20] Elaziz Mohamed Abd, Hosny Khalid M, Selim IM. Galaxies image classification using artificial bee colony based on orthogonal Gegenbauer moments. Soft Comput 2019;23(19):9573–83.
[21] Kashkari Bothayna SH, Syam Muhammed I. Fractional-order Legendre operational matrix of fractional integration for solving the Riccati equation with fractional order. Appl Math Comput 2016;290:281–91.
[22] Xiao B, Li L, Li Y, Li W, Wang G. Image analysis by fractional-order orthogonal moments. Inf Sci 2017;382–383:135–49.
[23] Zhang H, Li Z, Liu Y. Fractional orthogonal Fourier-Mellin moments for pattern recognition. In: The proceedings of Chin conf pattern recognit. Springer; 2016. p. 766–78.
[24] Benouini Rachid, Batioua Imad, Zenkouar Khalid, Zahi Azeddine, Najah Said, Qjidaa Hassan. Fractional-order orthogonal Chebyshev moments and moment invariants for image representation and pattern recognition. Pattern Recogn 2019;86:332–43.
[25] Faires JD, Burden RL. Numerical methods. third ed. Brooks Cole Publication; 2002.
[26] Hosny Khalid M, Darwish Mohamed M. A kernel-based method for fast and accurate computation of PHT in polar coordinates. J Real-Time Image Proc 2019;16(4):1235–47.
[27] Camacho-Bello C, Padilla-Vivanco A, Toxqui-Quitl C, Báez-Rojas JJ. Reconstruction of color biomedical images by means of quaternion generic Jacobi-Fourier moments in the framework of polar pixel. J Med Imaging 2016;3(1):014004.
[28] Hosny KM, Darwish MM. Feature extraction of color images using quaternion moments. In: Hassaballah M, Hosny KM, editors. Studies in Computational Intelligence, 804. p. 141–67.
[29] Sheng Y, Shen L. Orthogonal Fourier-Mellin moments for invariant pattern recognition. J Opt Soc Am A 1994;11(6):1748–57.
[30] Nene SA, Nayar SK, Murase H. Columbia object image library (COIL-20); 1996. Technical report CUCS-005-96.
[31] Lazebnik S, Schmid C, Ponce J. Semi-local affine parts for object recognition. Proceedings of the British machine vision conference, 2. p. 959–68.